arXiv:1208.2468v2 [cond-mat.supr-con] 29 Oct 2012

Origin of pressure induced second superconducting dome in $A_y\mathrm{Fe}_{2-x}\mathrm{Se}_2$ [A=K, (Tl,Rb)]

Tanmoy Das[1], and A. V. Balatsky[1,2]
[1]*Theoretical Division, Los Alamos National Laboratory, Los Alamos, New Mexico 87545 USA.*
[2]*Center for Integrated Nanotechnology, Los Alamos National Laboratory, Los Alamos, New Mexico 87545 USA.*
(Dated: October 30, 2012)

Recent observation of pressure induced second superconducting phase in $A_y\mathrm{Fe}_{2-x}\mathrm{Se}_2$ [A=K, (Tl,Rb)] calls for the models of superconductivity that are rich enough to allow for multiple superconducting phases. We propose the model where pressure induced changes in Fermi surface topology lead to appearance of the hole pocket at Γ point at high pressure. We develop low-energy effective model, derived from first-principles band-structure calculation, to suggest the phase assignment where low pressure superconducting state with no hole pocket at Γ point is a nodeless d-wave state. It evolves into a $s^{\pm}$ state at higher pressure when the Fermi surface topology changes and hole pocket appears. We analyze the pairing interactions using five band tight binding fitted band structure and find strong pairing strength dependents on pressure. We also evaluate the energy and momentum dependence of neutron spin resonances in each of the phases as verifiable predictions of our proposal.

PACS numbers: 74.70.Xa, 74.20.Rp, 74.25.Jb, 74.40.-n

High$-T_c$ superconductivity often occurs when the system is driven from its pristine phase to the verge of magnetic quantum critical point via external controlled parameters such as chemical doping, magnetic field or pressure (P) in most of the cuprates, heavy fermions, pnictides, and organic superconductors. However, several recent breakthrough discoveries of a second superconducting (SC) dome $-$ completely isolated or slightly connected to the first SC dome $-$ without the intervention of any competing order as a function of P in several families of high-T_c superconductors,[1–3] and/ or extreme chemical doping in $\mathrm{KFe_2As_2}$,[4] $\mathrm{LaFeAsO}_{1-2}\mathrm{H}_x$[5] or strain[6] have questioned this expectation. Much higher optimal T_c value than that of the first dome, as well as a substantial increase in electronic mass with P as obtained in iron-based compounds suggest an interesting and exotic phenomena of superconductivity along this tuning axis. It is notable that in stochiometric $\mathrm{SrFe_2As_2}$, a SC dome appears both as a function of P,[7] as well as crystallographic strain[6] near the quantum critical point of spin-density wave, as often observed in other high-T_c superconductors, further supporting the notion that the P induced superconductivity is unconventional. In this letter, we present a model that allows us to capture the onset of the second SC phase with different pairing symmetry as a function of P.

Our approach is based on the weak or intermediate coupling scenario in which the shape of the Fermi surface (FS) topology plays a key role in creating pairing instability at the 'hot-spot'.[8] For such case Cooper pairing arises from repulsive interaction with sign-reversal pairing symmetry constrained by the FS topology and crystal symmetries. This theoretical framework consistently describes $d-$wave pairing in cuprates,[8] and Ce-based heavy fermions,[9] $s^{\pm}$-pairing in iron-pnictides and chalcogenides,[10] and nodeless d-wave in $A_y\mathrm{Fe}_{2-x}\mathrm{Se}_2$ [A=K,Cs, Rb,(Tl,Rb), (Tl,K)] families.[11–13]

Here, we focus on the latter family in which a second isolated dome is observed, as shown Fig. 1(a) (reproduced from Ref. 14). In an analogous 122 compound $\mathrm{BaFe_2As_2}$,

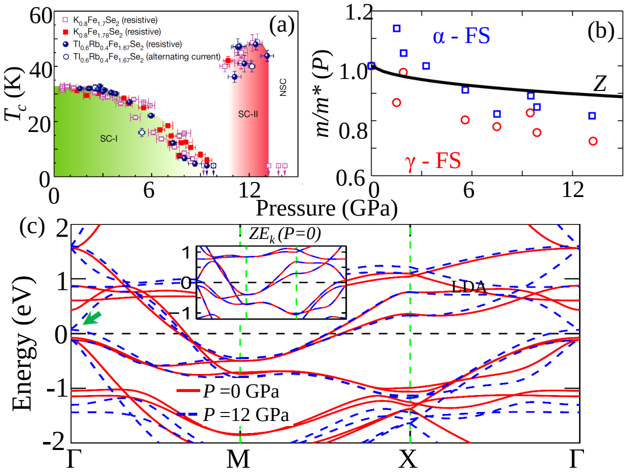

FIG. 1. (Color online) (a) Experimental phase diagram of T_c vs. P for several $A_y\mathrm{Fe}_{2-x}\mathrm{Se}_2$ systems, reproduced from Ref. 3. (b) Mass renormalization for hole-pocket (α-FS) and electron pocket (β-FS) for a related iron-pnictide compound $\mathrm{BaFe_2As_2}$, deduced from quantum oscillation measurements (symbols).[14] The experimental data are normalized to their values at $P=0$. Theoretical results of mass renormaliztion factor $Z=m/m^*$ for $A_y\mathrm{Fe}_{2-x}\mathrm{Se}_2$ compound (see text) plotted in solid line. (c) *Ab-inito* band structure of $\mathrm{KFe_2Se_2}$ at two representative Ps using TB-LMTO method (see text). *Inset:* Bands at $P=0$ (solid line) is multiplied by $Z=0.9$ which matches well with that for P=12 GPa, affirming the fact that P increases effective mass in this system as seen in experiment in (b).

it is established that the effective band mass, m^*, gradually increases as a function of P, see the plot of $1/m^*$ in Fig. 1(b). Constrained by these experimental facts we postulate that uniform P renormalizes the electronic structure, as also shown in first-principles calculations,[15] and thereby affects the FS topology. In $A_y\mathrm{Fe}_{2-x}\mathrm{Se}_2$ systems, both first principles calculation and angle-resolved photoemission spectroscopy (ARPES) have demonstrated that a hole-pocket lies slightly below the Fermi level (E_F) at ambient P. With band renormalization this hole pocket appears on the FS at some critical P, and the overall FS topology changes from only electron-pockets at $P = 0$ to the coexisting electron and hole pocket as in pnictides. This topological FS transition induces a crossover from FS nesting along diagonal $\boldsymbol{Q}_1 \to (\pi, \pi)]$ direction to along zone direction $\boldsymbol{Q}_2 \to (\pi, 0)/(0, \pi)$ which makes a pairing symmetry transition from nodeless d-wave to $s^{\pm}$-pairing.

We explore these postulates via first-principle band structure and pairing eigenvalue calculations within random-phase approximation (RPA). The first-principles calculation is performed within the atomic sphere approximation by using the TB-LMTO code.[16, 17] For a given P, the uniform volume contraction is evaluated using Birch-Murnaghan equation of state[18] formalism (given below). The key here is to optimize the Se atomic position with respect to the Fe plane by minimizing total energy at each P. We find $z_{Se} = 0.3452c$ at $P = 0$ GPa and $z_{Se} = 0.351c$ at $P = 12$ GPa. The obtained band structure in Fig. 1(c) shows that at $P =$12 GPa, the bands are renormalized by $Z \sim 0.9$ (see inset) which allows the hole-pockets to appear on the FS. Therefore the dominant FS instability arises along $\boldsymbol{Q}_2$ at a critical value of interaction U, and thus $s^{\pm}$ pairing with large coupling constant commences. We also semi-quantitatively reproduce the phase diagram of the d and $s^{\pm}$-pairings within the conditions for best nestings along each channels.

Formalism:- To grasp further insight into how P modifies electronic structure and also to enable adding correlations for pairing symmetry calculations, we derive a low-energy five-bands tight-binding (TB) formalism[12] to include pressure effect. The TB hopping integrals t_i in a given crystal is defined as $t = \langle\Psi|V_c|\Psi\rangle$, V_c is Coulomb interaction between lattice and electron, implying that $t_i(P)/t_i(0) \propto V(P)/V_0$, where $t_i(P)$ and $V(P)$ are the TB parameters and lattice volume at any given P P, and $t_i(0)$ and V_0 are their corresponding values at ambient P. For simplicity, we take $t_i(P)/t_i(0) \sim V(P)/V_0 \approx m/m^* = Z$, for all bands. From the value of Z or more strictly from the volume ratio, we can obtain the value of P using Birch-Murnaghan equation of state[18]

$$P = \frac{3B}{2}\left(x^{7/3} - x^{5/3}\right)\left[1 - \frac{3}{4}(4 - B')(x^{2/3} - 1)\right], \quad (1)$$

where $x = V_0/V = 1/Z$, and B, B' are the bulk modulus and its P derivative. To match the optimal doping of the second T_c dome with the experimental value we find $B \approx B'P = 67$ GPa, which is close to the experimental value of B=64 GPa.[19] Since Z renormalizes the TB hopping parameters only, not the entire bands, Fermi level adjustment is necessary at each value of P to keep the number of electron constant. We compute the Fermi level self-consistently, beyond a simple rigid band shift approximation, by integrating the density of state in the filled state as $n = 1/N\sum_{\boldsymbol{k},i=1-5}\int d\omega\delta(\omega - ZE^i_{\boldsymbol{k}})$, where $E^i_{\boldsymbol{k}}$ is the dispersion for i^{th} band. Our finding of crucial importance is that P can enable significant FS topological change even with fixed number of electrons. In what follows, the Luttinger volume, $V_L = 1/N\sum_{k_F,i}\delta(E^i_{\boldsymbol{k}_F})$ of all FSs changes as a function of P but the ratio $n = V_L/Z$ remains constant. This is due to the fact that, unlike in a Fermi liquid picture, here Z only renormalizes the dispersions, not the spectral function.

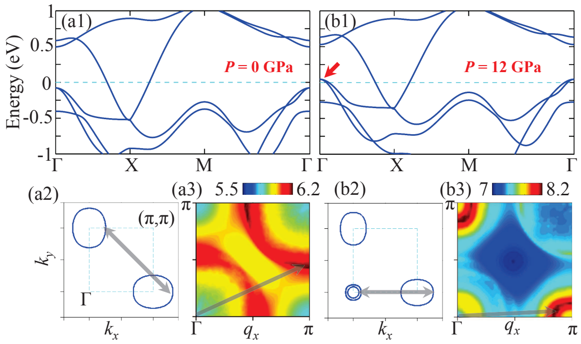

FIG. 2. (Color online) (a1-a3) TB bands and real-part of susceptibility at zero energy at ambient P. (b1-b3) Same but at $P = 12$ GPa and $Z = 0.9$. (a1), (b1) Self-consistently evaluated bands along high-symmetry lines in 1 Fe unit cell notation[12] at two P values. (a2), (b2) Corresponding FS topologies. (a3), (b3) Static susceptibilities plotted in the $\boldsymbol{q} = 0$-plane. Arrows depict the leading nesting directions.

Figure 2 reveals the evolution of electronic states at ambient P and at P=12 GPa. At $P = 0$, the hole pockets lies at 60 meV below the Fermi level (E_F) at Γ-point, as is also seen in angle-resolved photoemission spectroscopy (ARPES) data.[20] In this case, the presence of electron pockets at X-points (in 1 Fe per unit cell notation) is well established.[20–22] With the uniform band renormalization by $Z = 0.9$ at $P = 12$GPa, according to Eq. 1, we find that two concentric hole pockets are fully formed on the FS as seen from Figs. 2(b1) and 2(b2).

To determine the dominant nesting 'hot-spot', we perform multiband suscetibility calculation using full orbital overlap matrix-element effect. The many-body correction is incorporated within RPA via explicitly including intraorbital interaction U, interorbital interaction V, Hund's coupling $J > 0$ and the pair hopping energy J'. The full orbital components of interaction tensors U_s for spin RPA susceptibility and U_c charge RPA susceptibility are defined in Ref. [23] and the details of the calculation can, for example, be found in Refs. [11, 13, 24, 25]. We plot the static spin RPA susceptibility (trace of the susceptibility tensor) at the two representative Ps in Fig. 2(a3) for $P = 0$ and in Fig. 2(b3) for $P = 12$ GPa. As expected, the dominant nesting in the former case is aligned along the inter-electron-pocket direction [consistent with earlier calculation in Refs. [11–13]]. On the other hand at $P = 12$GPa, the dominant nesting changes to $\boldsymbol{Q}_2 \to (\pi, 0)$ between electron and hole pockets, as obtained for many iron-pictide superconductors.[10, 24]

Next we evaluate the effective pairing vertex in the singlet channel for scattering between two FSs i, j within spin and charge fluctuation exchange approximation[25]:

$$\hat{\Gamma}(\boldsymbol{k},\boldsymbol{k}') = \frac{1}{2}\Big[3\hat{U}_s\hat{\chi}_s(\boldsymbol{k}-\boldsymbol{k}')\hat{U}_s - \hat{U}_c\hat{\chi}_c(\boldsymbol{k}-\boldsymbol{k}')\hat{U}_c + \frac{1}{2}(\hat{U}_s+\hat{U}_c)\hat{\chi}_0(\boldsymbol{k}-\boldsymbol{k}')(\hat{U}_s+\hat{U}_c)\Big]. \quad (2)$$

The pairing strength for gap functions $g(\boldsymbol{k})$ is then determined by solving the eigenvalue problem[24]:

$$\lambda_{ij}[g] = -\frac{\oint_{C_i}\frac{dk}{v_F(k)}\oint_{C_j}\frac{dk'}{v_F(k')}g(\boldsymbol{k})\Gamma_{ij}(\boldsymbol{k},\boldsymbol{k}')g(\boldsymbol{k}')}{(2\pi)^2\oint_{C_j}\frac{dk}{v_F(k)}[g(\boldsymbol{k})]^2}. \quad (3)$$

Here the line integrals over C_i are performed on each FS loops, and v_F is the Fermi velocity. The key point of Eq. 3 is that if the gap function $g(\boldsymbol{k})$ possesses opposite sign at $\boldsymbol{k}$ and $\boldsymbol{k}'$, mediated by a large peak in Γ at the 'hot-spot' $\boldsymbol{q} = \boldsymbol{k} - \boldsymbol{k}'$. Based on this framework, we now study the evolution of λ for $g(\boldsymbol{k}) = \cos k_x - \cos k_y$ for $d_{x^2-y^2}$ and $g(\boldsymbol{k}) = \cos k_x \cos k_y$ for $s^{\pm}$-pairing channels (in the 1 Fe per unit cell notation) as a function of P in Figs. 3 and 4 (in 2 Fe per unit cell, the form of the pairing structure, i.e. $g(\boldsymbol{k})$ transforms by the same unitary transformation as the FS so that the macroscopic properties such as nodeless and isotropic gap structure remains same in any notation[13, 26]). To understand the origin of the pairing symmetry transition in details, we study each intra- and inter-band components of λ_{ij} in Fig. 3 at two representative Ps. These results confirm our initial assumption.

For $d_{x^2-y^2}$-wave pairing at $P = 0$ in Fig. 3(a) and at $P = 12$ GPa in Fig. 3(b), we obtain $\lambda > 0$ and < 0, respectively. This can be understood from the corresponding FS topological changes. At $P = 0$, the two electron pockets at $(\pi, 0)$ and $(0, \pi)$ posses opposite sign of SC gap, and this phase is supported by nesting along $\boldsymbol{Q}_1 \rightarrow (\pi, \pi)$, as deduced in Fig. 2(a3).[11–13] So we get $\lambda_{\gamma-\gamma} > 0$. But as the dominant 'hot-spot' changes to $\boldsymbol{Q}_2 \rightarrow (0, \pi)$ at $P = 12$ GPa, positive $\lambda_{\gamma-\gamma}$ component is overturned by large negative $\lambda_{\alpha-\gamma}$ and $\lambda_{\beta-\gamma}$ components being supported by $\boldsymbol{Q}_2$ 'hot-spot' without sign-reversal of $g(\boldsymbol{k})$. Therefore, the total λ becomes negative, making $d_{x^2-y^2}$ pairing unstable at this P. For $s^{\pm}-$pairing, the situation is reversed in that $\lambda_{\gamma-\gamma} < 0$ at all values of P, but $\lambda_{\alpha/\beta-\gamma} > 0$. It is important to note that due to the presence of two hole pockets α and β, the total value of λ becomes positive and large at some critical value of P, otherwise, $s^{\pm}$-pairing would have been favorable.

In Fig. 4, we show the full P and interaction U dependence of the total pairing strengh λ, and the corresponding calculated T_c. The d-wave pairing survives upto $P \sim 5$ GPa, slightly less than the termination point of the first SC shown in Fig. 1(a). Of course, these quantitative consistencies rely strongly on the exact shape of FS topology and the value of bulk modulus B used in Eq. 1. We focus on fitting B so that the optimum T_c for the second dome match with the experimental value of P. With a separation of about 1-2 GPa, we find that the $s^{\pm}-$pairing channel appears abruptly for a large range of U. Although we obtain an optimum λ as a function of P at which the FS nesting between α/β to γ is strong for all values of U considered, it survives to a larger P range than the experimental data of $K_{0.8}Fe_{1.7}Se_2$.[3] However, for other samples within the same family, new data shows that T_c in the second dome is very much P independent and survives up to P as large as 40 GPa measured so far.[27]

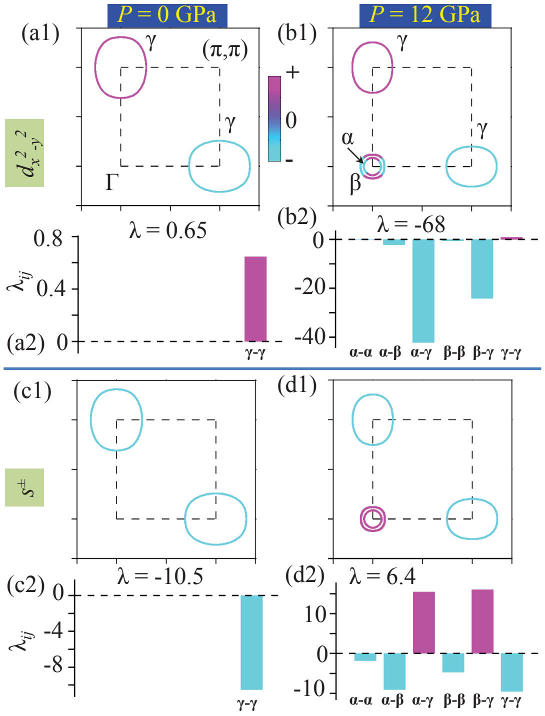

FIG. 3. (Color online) Evolution of different intra- and inter-band pairing eigenvalues, λ_{ij}, at two representative Ps (different columns) and pairing symmetries (different rows). Color coding on the FS in (a1), (b1), (c1), and (d1) gives the variation and sign of SC gaps on each FS pockets. At $P = 0$ (left column), the pairing eigenvalue arising from nesting between two electron-pockets is positive for d-wave, and negative for $s^{\pm}$pairing, indicating that the former pairing is stable here. At $P = 12$ GPa, the strong negative value of $\lambda_{\alpha-\gamma}$ and $\lambda_{\beta-\gamma}$, governed by same sign of SC gap for d-wave pairing connected by dominant 'hot-spot', yields total $\lambda < 0$, and thus unstable pairing. For $s^{\pm}$-pairing at this P, despite the presence of several negative values of λ, the dominant 'hot-spot' connects sign-reversal SC gap between two electron and two hole pockets, leading to total $\lambda > 0$. If one of the hole-pocket disappears, $s^{\pm}$-pairing will become unlikely in this case.

We compute T_c using standard McMillan's formula[28]

$$T_c = \frac{\omega_D}{1.20}\exp\left(-\frac{1.04(1+\lambda)}{\lambda - \mu^*(1+0.62\lambda)}\right), \quad (4)$$

With a value of pseudopotential $\mu^* = 0.1$ and Debye temperature ω_D=175 K, we obtain optimum T_c ~38 K and $T_c \sim 47$ K for the first and second dome, respectively, for $U = 1.2$, which are close to the experimental values of 37 K and 48 K. It is obvious that the absolute value of T_c depends on the interaction parameter, however, the ratio between the optimum value at two domes is always maintained. Interestingly, we find that the computed T_c for the second dome is even flatter

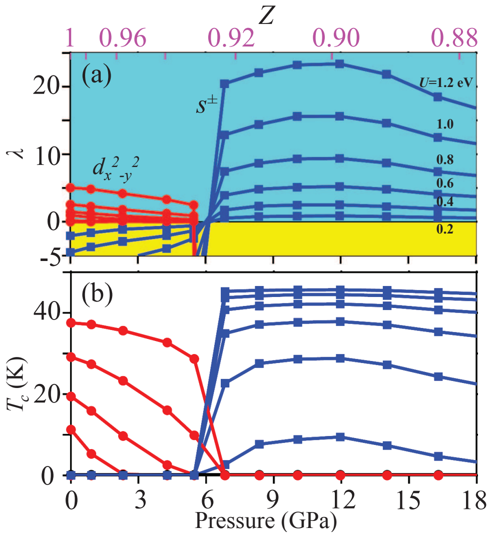

FIG. 4. (Color online) (a) Evolution of total pairing eigenvalues for d-wave (solid circles) and $s^{\pm}$-pairing as a function of P for various values of U. The horizontal axis at the top of the plot gives the computed value of Z from Eq. 1. The color shadings separates the negative and positing eigenvalue regions. (b) Computed values of T_c, using Macmillan's formula in Eq. 4, are plotted as a function of P. The persistent of T_c in the second SC region upto high P is observed in a number of materials other than $K_0.8Fe_{1.7}Se_2$.[27]

than that for λ and thus agrees well with the new data.[27]

Relating the glue function to the spin-resonance mode that appears in the SC state, we expect a resonance around $\omega_D \sim$ 15 meV ($\sim$ 174 K) at the optimum P. The phenomena of spin-resonance in the SC state is well known[8–11, 24] and is essentially similar to the condition for obtaining positive pairing eigenvalue λ as discussed above: Given that the sign reversal of SC gap is connected by momentum transfer $\boldsymbol{q}$ a spin-resonance appears at an energy $\omega(\boldsymbol{q}) \sim |\Delta(\boldsymbol{k})| + |\Delta(\boldsymbol{k}+\boldsymbol{q})|$ (RPA correction shifts the mode to a slightly lower energy). We compute the spin-resonance spectra at the same representative P values as in Figs. 2 and 3 for d-wave and $s^{\pm}$-pairing and the results are shown in Fig. 5. We immediately see that for d-wave pairing we get a nearly commensurate spin-resonance mode at $\omega/2\Delta \sim 0.8$, while it becomes incommensurate and shifts to higher energy for the $s^{\pm}$-pairing at higher P. Although, ARPES and INS measurements are difficult to perform under P, neutron diffraction experiment can be done here to test the changes of $\boldsymbol{Q}$ vector as a function of P to verify our results.

In conclusion, we present an analysis of pressure evolution of pairing interaction in $A_y\mathrm{Fe}_{2-x}\mathrm{Se}_2$ family of superconductors. We argue that observed two SC domes can be naturally explained by changes in FS topology driven by mass enhancements. At lower P, we expect no Γ-point hole pocket on the FS, and therefore d-wave SC state.[29] Upon increase in P, we expect two hole pockets to develops at Γ-point, leading to pairing symmetry transition to $s^{\pm}$-pairing. Therefore, the natural outcome of our analysis is that there are two distinct SC states, nodeless d-wave at smaller P and $s^{\pm}$-pairing at higher P that can be realized in these materials. To test these predictions, we suggest to use magnetic field dependent tunneling spectroscopies to investigate gap changes.[30] Neutron scattering and neutron diffraction measurements would reveal the distinct pattern of spin resonance and nesting properties in these phases.

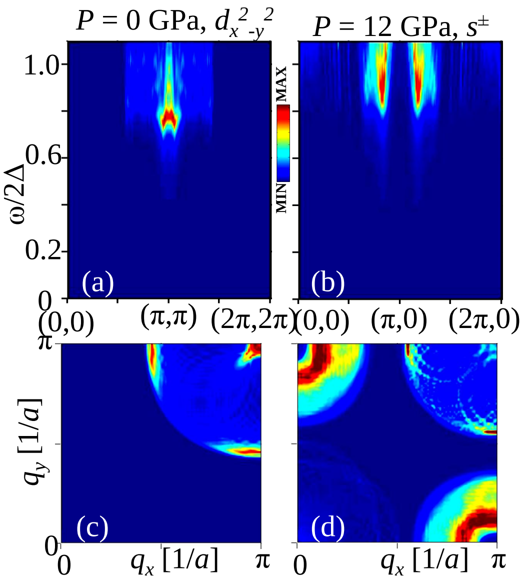

FIG. 5. (Color online) (a) Spin excitation spectrum along zone diagonal direction as a function of energy for $P = 0$, and d-wave pairing. (b) Same but along zone boundary direction at $P = 12$ GPa and $s^{\pm}$-pairing. (c)-(d) Constant energy cuts at their corresponding resonance energy values.

This work was supported, in part, by UCOP-TR27 and by Los Alamos National Laboratory, of the US Department of Energy under Contract DE-AC52-06NA25396, and benefited from the allocation of supercomputer time at NERSC.

---

[1] H. Q. Yuan *et al.*, Science **302**, 2104 (2003).
[2] X. J. Chen *et al.*, Nature **466**, 950 (2010).
[3] L. Sun *et al.*, Nature **483**, 67 (2012).
[4] K. Sasmal, Phys. Rev. Lett. **101**, 107007 (2008).
[5] S. Iimura *et al.*, arXiv:1207.0583, to appear in Nat. Comm. (2012).
[6] S. R. Saha *et al.*, Phys. Rev. Lett. **103**, 037005 (2009).
[7] H. Kotegawa, H. Sugawara, and H. Tou, J. Phys. Soc. Jpn. **78** 013709 (2009).
[8] D. J. Scalapino, E. Loh, Jr., and J. E. Hirsch, Phys. Rev. B **34**, 8190 (1986).
[9] A. V. Chubukov and L. P. Gor'kov, Phys. Rev. Lett. **101**, 147004 (2008).
[10] I. I. Mazin, D. J. Singh, M. D. Johannes, and M. H. Du, Phys. Rev. Lett. **101**, 057003 (2008).
[11] T.A. Maier, S. Graser, P.J. Hirschfeld, and D.J. Scalapino, Phys. Rev. B **83**, 100515(R) (2011).
[12] Fa Wang *et al.*, Europhy. Lett. **93**, 57003 (2011).

[13] T. Das, and A. V. Balatsky, Phys. Rev. B **84**, 014521 (2011).
[14] D. Graf *et al.*, Phys. Rev. B **85**, 134503 (2012).
[15] A. Ciechan *et al.*, Acta Physica Polonica A **121**, 820 (2012).
[16] O.K. Andersen, Phys. Rev. B **12**, 3060 (1975).
[17] O.K. Andersen, O. Jepsen, Phys. Rev. Lett. **53**, 2571 (1984).
[18] F. Birch, Phys. Rev. **71**, 809 (1947).
[19] A. L. Ivanovskii, Physica C, **471**, 409-427 (2011).
[20] Y. Zhang *et al.*, Nat. Mat. **10,** 273-277 (2011).
[21] T. Qian *et al.*, Phys. Rev. Lett. **106**, 187001 (2011).
[22] D. Mou *et al.*, Phys. Rev. Lett. **106**, 107001 (2011).
[23] The spin and charge RPA susceptibilities are defined as $\hat{\chi}_s = \hat{\chi}_0/(1-\hat{U}_s\hat{\chi}_0)$ and $\hat{\chi}_c = \hat{\chi}_0/(1+\hat{U}_s\hat{\chi}_0)$, where $\hat{\chi}_0$ is the non-interacting susceptibility tensor, and $\hat{U}_{s/c}$ are spin and charge interaction vertex, defined in the orbital basis, see Ref. [25].
[24] S. Graser, T. A. Maier, P. J. Hirschfeld, and D. J. Scalapino, N. J. Phys. **11**, 025016 (2009).
[25] T. Takimoto, T. Hotta, and K. Ueda, Phys. Rev. B **69**, 104504 (2004).
[26] T. Das, and A. V. Balatsky, Phys. Rev. B **84**, 115117 (2011).
[27] X.-J. Chen *et al.* (unpublished); private communication.
[28] W. L. McMillan, Phys. Rev. **167** 331 (1968).
[29] X.-P. Wang *et al.*, arXiv:1205.0996.
[30] T. Hanaguri *et al.*, Science **328**, 474 (2010).